Global conformal diagram of a black hole with angular momentum

Marcos A. Argañaraz[†] and Osvaldo M. Moreschi[†‡]

[†] *Facultad de Matemática Astronomía, Física y Computación (FaMAF), Universidad Nacional de Córdoba,*

[‡] *Instituto de Física Enrique Gaviola (IFEG), CONICET, Ciudad Universitaria, (5000) Córdoba, Argentina.*

December 21, 2022

We present the first explicit global conformal diagram of Kerr spacetime and discuss some implications on the causal structure.

For this construction we use a new double null coordinate system for Kerr spacetime, which we have recently presented. These null coordinates are smooth everywhere and are naturally adapted to the horizons and to the null infinities.

In this setting there naturally appears a family of spheres that are parameterized by r_s, which are the intersections of both null coordinates, and r_s can be thought of as the extension of the tortoise coordinate for the Kerr spacetime.

1 Introduction

The formation of a black hole is normally thought of as the result of the collapse of a previous system. All observed compact objects have angular momentum; so that it is expected that any possible collapse to a black hole state will include some final angular momentum. Then, since the stationary axisymetric vacuum solution of the Hilbert-Einstein equations with angular momentum is the Kerr geometry[1]; it is natural to think of this metric as one of the most important in the study of general relativity.

Very recently these geometries have also acquired observational importance, since the direct observation of gravitational waves[2, 3]. Most of the observations correspond to binary black hole systems, whose final state is supposed to be represented by a remaining black hole with angular momentum. For this reason the Kerr metric becomes of relevance in this framework; since perturbations of this geometry could be used to describe the late time behavior of those systems.

The recent presentation of the first image ever generated[4] of a black hole is also related to this geometry. At the time of writing the Event Horizon Telescope(EHT) Collaboration has presented a second image, in this case of the supermassive black hole in the center of our own galaxy[5]. The models employed by the EHT Collaboration to create the image make use of this geometry, as also do other approaches to construct these type of images[6].

To have a deep physical understanding of a spacetime, it is crucial to know its causal structure. The use of null coordinates together with conformal diagrams were very useful tools for these purposes. They help to understand the nature of black holes horizons and are widely used in a variety of studies.

In spherically symmetric spacetimes, it is natural to consider diagrams in which each point corresponds to one of the spheres of symmetries, leading to the usual causal diagrams of the spacetime, as for example those presented in [7]. For the Schwarzschild case the use of the tortoise coordinate given by $r_* = r + 2m \ln(\frac{r}{2m} - 1)$ was useful.

For a black hole with angular momentum, the situation is much more delicate. In the sixties Carter[8] was able to study in detail the 'complete analytic extension of the symmetry axis of Kerr spacetime', and he presented the now celebrated conformal diagram at the symmetry axis of this spacetime. These type of diagrams are also reproduced in classic textbooks[9]. At the end of his article Carter conjectured that it was 'probable that the basic topological properties of the 4-dimensional manifold' were essentially the same. Yet, before the present article, there were no publications of an explicit construction of global conformal diagrams of a black hole with angular momentum. In many articles and presentations, Carter diagrams are used as if the Carter conjecture where true without presenting any argument for its support. The conformal diagram we are presenting in this article is then a useful tool to tackle questions as the above Carter conjecture; which we explore later in this work.

Two dimensional conformal, and therefore causal, diagrams are a very useful tool for visualizing the structure of the spacetime. Could one extend the usual two dimensional conformal diagrams of Schwarzschild geometry, based on Kruskal coordinates, to the case of a black hole with angular momentum? Yes, fortunately, we have recently constructed a pair of null coordinates that allows us to extend those techniques to the Kerr geometry.

The term 'conformal diagram' can be given slightly different meanings; in particular it is rather easy to construct a conformal diagram out of a static 2-dimensional Lorentzian spacetime[10], since one can readily find a pair of null functions. Then in particular one could compactify the spacetime to obtain a conformal diagram of it. But in our case we use the denomination 'conformal diagram' in a 4-dimensional sense; that is, one is hoping that generic points in the 4-dimensional spacetime can be represented in the conformal diagram. In order to fix the discussion we define: *global conformal diagrams* of a 4-dimensional spacetime as 2-dimensional graphs, in which lines at 45° represent constant null functions, and generic points of the spacetime can be mapped through a mathematical function to the 2-dimensional graphs. It is then customary to use compactifications so that infinities can also be drawn in these diagrams. Typical examples of diagrams that embody this definition are the graphs (i) and (ii) of figure 24 of Hawking and Ellis textbook[11]. Instead, the graphs shown in the same reference in figure 28, for Kerr spacetime, do not clasify as 'global conformal diagrams' since they refer to specific points along the axis of symmetry. In this work we provide for the first time an explicit construction of global conformal diagrams of Kerr spacetime.

A natural question that arises is whether the conformal diagrams that we present in this article provide any advantage for the analysis of the images of the observed black holes, the answer to which needs for some explanation. To begin with, the standard representation one has in mind as the source for the astrophysical system that generates the images that EHT Collaboration have published, is that surrounding material close to the black holes emits electromagnetic radiation that is captured by the radiotelescopes. That is, all the physical observed system is thought to be located outside the event horizon. From this point of view then our contribution would not add to the known structure, outside the horizon, of black holes with angular momentum. A second representation that one could consider is to include the possibility that the astrophysical black hole has also a past event horizon, and that null geodesics could reach us from past regions of this horizon. In this case, our construction could help in analysing the behavior of those geodesics, by providing the opportunity to depict them in our diagrams. Nonetheless, the general belief is that astrophysical black holes are always in the presence of surrounding material that would complicate this picture in several ways; inducing us to take the first standard representation, considered above, as the realistic one.

Note that one of the great benefits of the construction presented here is that now one can easily make any computation across the event horizon and the Cauchy horizon, either for particles or fields. This contributes on the physical studies in a broad spectrum of topics and results.

We use the standard notation for regions of type I, II and III to correspond respectively to the situations[8] $r > r_+$, $r_+ > r > r_-$ and $r_- > r$.

We will show below that the noncausal zone in region III can not be represented in global conformal diagrams. We can only draw its boundary. Throughout this work we assume the standard situation $a^2 < m^2$; where the geometric parameters are defined below in the metric.

In what follows we present the basic tools that are used to construct the most general explicit conformal diagram of a black hole with angular momentum. In section 2 we review the basic geometry and definition of a pair of null coordinates, that are adapted to the horizons. The null coordinates in regions II and III are presented in section 3. In section 4 we recall the conformal diagram at the axis of symmetry. With our construction, we are able in section 5 to present a numerically generated graph of three timelike curves in a conformal diagram. In section 6 we present graphs that depict the boundary of the noncausal region in Kerr spacetime. The conformal diagram of regions I, II and III is discussed in section 7 . An ending section is devoted to final comments.

2 The Kerr geometry

2.1 The basic pair of null coordinates

The Kerr metric in terms of Boyer-Lindquist[12] coordinates can be expressed as:

$$ds^2 = (1-\Phi)\,dt^2 + 2\,\Phi a \sin^2(\theta) dt d\phi - \frac{\Sigma}{\Delta} dr^2 - \Sigma d\theta^2 - \left(r^2 + a^2 + \Phi\, a^2 \sin^2(\theta)\right) \sin^2(\theta) d\phi^2; \tag{1}$$

with inverse

$$\left(\frac{\partial}{\partial s}\right)^2 = \frac{\Upsilon}{\Sigma\Delta}\left(\frac{\partial}{\partial t}\right)^2 + \frac{4amr}{\Sigma\Delta}\left(\frac{\partial}{\partial t}\right)\left(\frac{\partial}{\partial \phi}\right) - \frac{\Delta}{\Sigma}\left(\frac{\partial}{\partial r}\right)^2 - \frac{1}{\Sigma}\left(\frac{\partial}{\partial \theta}\right)^2 - \frac{\Delta - a^2\sin^2(\theta)}{\Sigma\Delta\sin^2(\theta)}\left(\frac{\partial}{\partial \phi}\right)^2; \tag{2}$$

where

$$\Sigma = r^2 + a^2\cos^2(\theta), \quad \Delta = r^2 + a^2 - 2mr, \quad \Upsilon = \left(r^2+a^2\right)^2 - \Delta a^2\sin^2(\theta), \quad \Phi = \frac{2mr}{\Sigma}; \tag{3}$$

and where m denotes de mass while the angular momentum of the black holes is given by $J = am$. In their work, Boyer and Lindquist were able to study the analytic extensions of the Kerr geometry.

Let us note for future reference that

$$g_{\phi\phi} = -\left(r^2 + a^2 + \Phi\, a^2\sin^2(\theta)\right)\sin^2(\theta) = -\frac{\Upsilon}{\Sigma}\sin^2(\theta); \tag{4}$$

that is, this component of the metric is proportional to Υ; which we will study below.

To build the outgoing congruence we make use of the Carter constant K on each geodesic, which in our construction becomes a function of the coordinates (r,θ). But often, it is useful to refer instead to a related scalar that we call $k(r,\theta)$ and is defined by:

$$K(r,\theta) = a^2\sin(\theta)^2 + k^2(r,\theta). \tag{5}$$

The details for the construction of the null congruence and the definition of the null coordinates are given in [13]; we here just recall some of the most important equations. These auxiliary scalars must satisfy the equation

$$\sqrt{(r^2+a^2)^2 - K\Delta}\,\frac{\partial K}{\partial r} \pm |_h\sqrt{K - \left(a\sin(\theta)\right)^2}\,\frac{\partial K}{\partial \theta} = 0; \tag{6}$$

with boundary condition

$$\lim_{r\to\infty} K = a^2\sin(\theta_\infty)^2; \tag{7}$$

where θ_∞ is the value of the coordinate θ at future null infinity; or equivalently

$$\frac{\partial k}{\partial \xi} = \frac{a^2\sin(\theta)\cos(\theta) + k\frac{\partial k}{\partial \theta}}{\sqrt{(1+\xi^2a^2)^2 - \xi^4\Delta\left(a^2\sin(\theta)^2 + k^2\right)}}; \tag{8}$$

where

$$\xi = \frac{1}{r}, \tag{9}$$

with boundary condition

$$\lim_{\xi\to 0} k = 0; \tag{10}$$

and we are assuming $k > 0$ in the northern hemisphere[13].

In our previous work [13] we have presented a pair of null functions that are smooth everywhere and therefore can be used as coordinates for the spacetime. Moreover, they are adapted to the horizons, as we will review here. These null functions were constructed in terms of particular congruences of null geodesics. We defined the outgoing congruence to be orthogonal to the center of mass sections[14, 15] at future null infinity. This construction has the advantage that it can be generalized to spacetimes, which are not exactly Kerr, but instead a perturbed spacetime that is decaying to a remaining black hole with angular momentum.

One can express the integral form of these functions in several ways[13], and we choose:

$$u(t,r,\theta,\phi) = t - r - \left(\frac{2mr_+}{r_+-r_-}\ln(\frac{r}{r_+}-1) - \frac{2mr_-}{r_+-r_-}\ln(\frac{r}{r_-}-1)\right) - \int_0^\theta k(r,\theta')\,d\theta'. \tag{11}$$

And for the other function we choose

$$v(t,r,\theta,\phi) = t + r + \left(\frac{2mr_+}{r_+-r_-}\ln(\frac{r}{r_+}-1) - \frac{2mr_-}{r_+-r_-}\ln(\frac{r}{r_-}-1)\right) + \int_0^\theta k(r,\theta')\,d\theta'. \tag{12}$$

Starting from the metric in Boyer-Lindquist coordinates (1), and expressing it in terms of the *center of mass null coordinates*, one obtains:

$$dt = \frac{dv+du}{2}, \tag{13}$$

$$dr = \left[\frac{(dv-du)}{2} - k\,d\theta\right]\frac{\Delta}{\sqrt{\mathcal{R}}}. \tag{14}$$

where $\mathcal{R} = (r^2+a^2)^2 - K\Delta$; from which, the metric is expressed as

$$\begin{aligned} ds^2 =& \frac{1}{4}\left(1 - \frac{2mr}{\Sigma} - \frac{\Sigma\Delta}{\mathcal{R}}\right)(du^2+dv^2) + \frac{1}{2}\left(1 - \frac{2mr}{\Sigma} + \frac{\Sigma\Delta}{\mathcal{R}}\right) du\, dv \\ &+ dv\left(\frac{2amr\sin^2(\theta)}{\Sigma}\, d\phi + \frac{\Sigma\Delta}{\mathcal{R}} k\, d\theta\right) + du\left(\frac{2amr\sin^2(\theta)}{\Sigma}\, d\phi - \frac{\Sigma\Delta}{\mathcal{R}} k\, d\theta\right) \\ &- \frac{\Upsilon\,\Sigma}{\mathcal{R}} d\theta^2 - \frac{\Upsilon}{\Sigma}\sin^2(\theta)\, d\phi^2. \end{aligned} \tag{15}$$

Similarly, the inverse metric can be expressed as:

$$\begin{aligned} \left(\frac{\partial}{\partial s}\right)^2 =& 4\,\frac{\Upsilon}{\Sigma\Delta}\left(\frac{\partial}{\partial u}\right)\left(\frac{\partial}{\partial v}\right) - \frac{1}{\Sigma}\left(\frac{\partial}{\partial\theta}\right)^2 + 2\left(\frac{\partial}{\partial u}\right)\left[\frac{2amr}{\Sigma\Delta}\left(\frac{\partial}{\partial\phi}\right) + \frac{k}{\Sigma}\left(\frac{\partial}{\partial\theta}\right)\right] \\ &+ 2\left(\frac{\partial}{\partial v}\right)\left[\frac{2amr}{\Sigma\Delta}\left(\frac{\partial}{\partial\phi}\right) - \frac{k}{\Sigma}\left(\frac{\partial}{\partial\theta}\right)\right] - \frac{\Delta - a^2\sin^2(\theta)}{\Sigma\Delta\sin^2(\theta)}\left(\frac{\partial}{\partial\phi}\right)^2. \end{aligned} \tag{16}$$

It is easy to verify that $\ell_a \equiv (du)_a$ and $\mathfrak{n}_a \equiv (dv)_a$ are null forms, which is consistent with our definition. We occasionally use Latin letters in this article to denote abstract indices.

2.2 Regular coordinates at the horizon

From observing the variation of the derivative of the Boyer-Lindquist coordinate ϕ with respect to the affine parameter[13] λ, one finds that ϕ has a divergent behavior as the horizon is approached. In order to avoid this bad behavior we choose to define

$$d\varphi_{\pm_{pf}} = d\phi - \pm_{pf}\frac{a}{\Delta}dr; \tag{17}$$

which has an integral expression given by

$$\varphi_{\pm_{pf}} = \phi - \pm_{pf}\frac{a}{2\sqrt{m^2-a^2}}\ln\left|\frac{r-r_+}{r-r_-}\right|; \tag{18}$$

where we are using the notation $(\pm_{pf} = +)$ for the choice p and $(\pm_{pf} = -)$ for the choice f. That is, φ_+ is well behaved as one approaches the past horizon H_p, and φ_- is well behaved as one approaches the future horizon H_f.

It can be proved[13] that the function $U = -\exp(-\kappa u)$ is well behaved across the future horizon H_f when $\kappa = \kappa_+$, where

$$\kappa_+ = \frac{(r_+ - r_-)}{2(r_+^2+a^2)} = \frac{\sqrt{m^2-a^2}}{2mr_+}; \tag{19}$$

which is customary referred to as the surface gravity of the black hole. In particular one can see that, near the horizon one has $U \propto \Delta$; where the proportionality factors are smooth functions on the horizon. In order to have a double null system that is smooth across the outer past event horizon we also define the null function V in a similar way; so that we have

$$U = -\exp(-\kappa_+ u), \tag{20}$$

and

$$V = \exp(\kappa_+ v). \tag{21}$$

Up to now, we have been studying the asymptotic behavior approaching the horizon from the outside region where $\lambda < \lambda_+$. In the inner region, $U > 0$ and one should use the relation

$$U = \exp(\kappa_+ u_{II}); \tag{22}$$

where u_{II} is the analogous inner version of the null coordinate u in the outer region.

Then, the metric becomes

$$
\begin{aligned}
ds^2 =& \frac{1}{4}\left(1-\frac{2mr}{\Sigma}-\frac{\Upsilon a^2\sin^2(\theta)+\Sigma^2\Delta}{\Sigma\mathcal{R}}-\frac{\pm_{pf}4mra^2\sin^2(\theta)}{\Sigma\sqrt{\mathcal{R}}}\right)\frac{1}{\kappa^2U^2}\,dU^2\\
&+\frac{1}{4}\left(1-\frac{2mr}{\Sigma}-\frac{\Upsilon a^2\sin^2(\theta)+\Sigma^2\Delta}{\Sigma\mathcal{R}}\pm_{pf}\frac{4mra^2\sin^2(\theta)}{\Sigma\sqrt{\mathcal{R}}}\right)\frac{1}{\kappa^2V^2}\,dV^2\\
&-\frac{1}{2}\left(1-\frac{2mr}{\Sigma}+\frac{\Upsilon a^2\sin^2(\theta)+\Sigma^2\Delta}{\Sigma\mathcal{R}}\right)\frac{1}{\kappa^2UV}\,dU\,dV\\
&+\left[\frac{\left(\Upsilon a^2\sin^2(\theta)+\Delta\Sigma^2\right)}{\Sigma\mathcal{R}}\pm_{pf}\frac{2mra^2\sin^2(\theta)}{\Sigma\sqrt{\mathcal{R}}}\right]\frac{k}{\kappa U}dU\,d\theta\\
&+\left[\frac{\left(\Upsilon a^2\sin^2(\theta)+\Delta\Sigma^2\right)}{\Sigma\mathcal{R}}-\frac{\pm_{pf}2mra^2\sin^2(\theta)}{\Sigma\sqrt{\mathcal{R}}}\right]\frac{k}{\kappa V}dV\,d\theta\\
&-\left(\frac{2amr\sin^2(\theta)}{\Sigma}\pm_{pf}\frac{\Upsilon a\sin^2(\theta)}{\Sigma\sqrt{\mathcal{R}}}\right)\frac{1}{\kappa U}\,dU\,d\varphi\\
&+\left(\frac{2amr\sin^2(\theta)}{\Sigma}-\pm_{pf}\frac{\Upsilon a\sin^2(\theta)}{\Sigma\sqrt{\mathcal{R}}}\right)\frac{1}{\kappa V}\,dV\,d\varphi\\
&-\left[\Sigma+\frac{k^2\left(\Upsilon a^2\sin^2(\theta)+\Sigma^2\Delta\right)}{\Sigma\mathcal{R}}\right]d\theta^2\\
&\pm_{pf}\frac{2\Upsilon a\sin^2(\theta)}{\Sigma\sqrt{\mathcal{R}}}k\,d\theta\,d\varphi-\frac{\Upsilon}{\Sigma}\sin^2(\theta)\,d\varphi^2,
\end{aligned}
\tag{23}
$$

where one has to consider $\kappa=\kappa_+$ and we are using the new angular coordinate φ.

The inverse metric can be expressed as:

$$
\begin{aligned}
\left(\frac{\partial}{\partial s}\right)^2 =& -4\kappa^2\frac{\Upsilon}{\Sigma\Delta}U\,V\left(\frac{\partial}{\partial U}\right)\left(\frac{\partial}{\partial V}\right)-\frac{2\kappa k}{\Sigma}\left[U\left(\frac{\partial}{\partial U}\right)+V\left(\frac{\partial}{\partial V}\right)\right]\left(\frac{\partial}{\partial\theta}\right)\\
&-\frac{2\kappa\,a\,U}{\Sigma\Delta}\left(2mr-\pm_{pf}\sqrt{R}\right)\left(\frac{\partial}{\partial U}\right)\left(\frac{\partial}{\partial\varphi}\right)+\frac{2\kappa\,a\,V}{\Sigma\Delta}\left(2mr\pm_{pf}\sqrt{R}\right)\left(\frac{\partial}{\partial V}\right)\left(\frac{\partial}{\partial\varphi}\right)\\
&-\frac{1}{\Sigma}\left(\frac{\partial}{\partial\theta}\right)^2-\frac{1}{\Sigma\sin^2(\theta)}\left(\frac{\partial}{\partial\varphi}\right)^2,
\end{aligned}
\tag{24}
$$

where $\kappa=\kappa_+$.

The determinant of the metric is given by

$$
g=-\frac{\Delta^2\Sigma^2\sin(\theta)^2}{4\kappa^4\mathcal{R}U^2V^2}. \tag{25}
$$

The future outer horizon H_f is reached following the incoming null geodesic congruence while the past outer horizon H_p is reached following the outgoing null geodesic congruence but to the past. The behavior of U and V near the horizon can be seen from the expression of the product of both functions, since one has

$$
UV=\frac{-\,e^{2\kappa_+\left(r+\int_0^\theta k(r,\theta')d\theta'\right)}\left(r_-\right)^{\frac{r_-}{r_+}}}{\left(r_+\right)\left(r-r_-\right)^{\frac{r_++r_-}{r_+}}}\,\Delta. \tag{26}
$$

From the definition of both functions, one can see that $U\approx\Delta$ at the future outer horizon H_f and $V\approx\Delta$ at the past outer horizon H_p.

Let us notice that each one-form dt_a and dr_a (normal to a surface t =constant, r =constant respectively) changes its causal character between region I and II, as we can see from their norms

$$
g^{ab}dt_adt_b=\frac{\Upsilon}{\Sigma\Delta}, \tag{27}
$$

$$
g^{ab}dr_adr_b=-\frac{\Delta}{\Sigma}. \tag{28}
$$

In region I where $\Delta>0$, we have that dt_a is timelike and dr_a spacelike. In region II where $\Delta<0$, we have that dt_a changes to spacelike and dr_a changes to timelike. In region III where $\Delta>0$, we have a similar situation as in region I.

One can see that something similar happens with

$$
\left(dr_s\right)_a=\frac{\sqrt{\mathcal{R}}}{\Delta}\,dr_a+k\,d\theta_a, \tag{29}
$$

which norm is

$$g^{ab}\,(dr_s)_a\,(dr_s)_b = -\frac{\Upsilon}{\Sigma\Delta}, \tag{30}$$

so that dr_s is spacelike in region I where $\Delta > 0$, and becomes temporal in region II where $\Delta < 0$. In order to keep the same causal meaning of the null functions u, v, we need to define new ones. There are several reasons that induce us to define the new coordinate r_s. The function r_s is the analog to the tortoise coordinate in Schwarzschild spacetime. These can be seen, as it already appears in the integral form of the coordinates u and v, in equations (11) and (12). It has the meaning of a function that is constant on the 2-surfaces that are the intersections of the hypersurfaces u =constant and v =constant. These 2-surfaces are topologically spheres, and are the natural closed surfaces that appear in our construction of the double null coordinate system. The coordinate r_s also has the convenient property that is constant in each point of the conformal diagrams we are presenting in this article. Note that, as we have explained in [13], r_s can explicitly be given in the exterior region by

$$r_s(r,\theta) = r + \frac{2mr_+}{r_+ - r_-}\ln(\frac{r}{r_+} - 1) - \frac{2mr_-}{r_+ - r_-}\ln(\frac{r}{r_-} - 1) + \int_0^\theta k(r,\theta')\,d\theta'. \tag{31}$$

This equation shows the relation between r_s with the standard Boyer-Lindquist coordinates (r,θ). If we call $r_{\rm KS}$ the Kerr-Schild radial coordinate, that is, $r^2_{\rm KS} = x^2_{\rm KS} + y^2_{\rm KS} + z^2_{\rm KS}$; then, we have to recall that $r^4 - (r^2_{\rm KS} - a^2)r^2 - a^2 z^2_{\rm KS} = 0$. Therefore, one could replace above the appearance of r with the corresponding functional relation $r(r_{\rm KS}, z_{\rm KS})$, to find the relation of r_s in terms of the radial Kerr-Schild coordinate. To have a qualitative comparison of the surfaces r_s =const., r =const. and $r_{\rm KS}$ =const. we have made the graph shown in figure 1; where we can see that for these parameters, the r_s =const. is located between the other two. We have

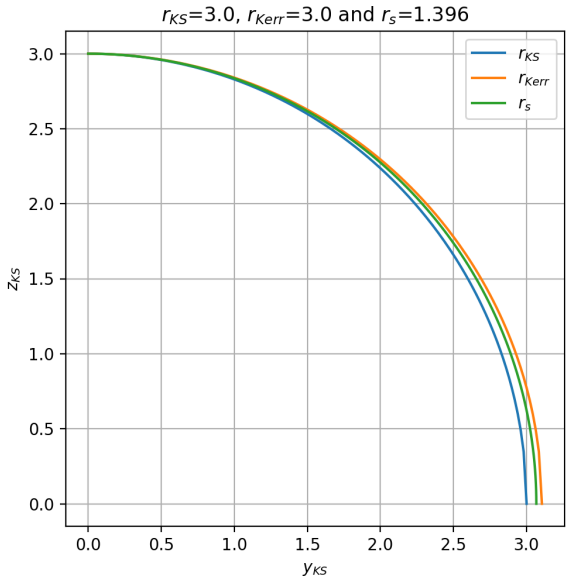

Figure 1: Comparison of different radial functions maintained constant, with respect to Kerr-Shild coordinates.

emphasized the Kerr coordinate[1] r with the notation $r = r_{Kerr}$ in this graph. Whenever necessary, to make an explicit numerical calculation, we assume $m = 1$ and $a = 0.8$. We have chosen the value of r to triple the mass, which taking into account that for our choice of parameters $r_+ = 1.6m$, one can see that it is smaller than double the value of r_+.

Before continuing with the other regions let us also note that $dv = du + 2dr_s$, so that, for example, the Kerr metric in the (u, r_s, θ, ϕ) coordinate system, can be obtained from (15) by this replacement; namely

$$\begin{aligned} ds^2 = &(1-\Phi)\,du^2 + 2\,(1-\Phi)\,du\,dr_s + 2a\sin^2(\theta)\Phi du\,d\phi + \left(1 - \Phi - \frac{\Sigma\Delta}{\mathcal{R}}\right)dr_s^2 + 2k\frac{\Sigma\Delta}{\mathcal{R}}dr_s\,d\theta \\ &+ 2a\sin^2(\theta)\Phi dr_s\,d\phi - \frac{\Upsilon\,\Sigma}{\mathcal{R}}d\theta^2 - \left(r^2 + a^2 + a^2\sin^2(\theta)\Phi\right)\sin^2(\theta)\,d\phi^2. \end{aligned} \tag{32}$$

[1] Although r is normally understood as the radial Boyer-Lindquist coordinate, it already appeared in the original paper[16] of Kerr.

It is probably worthwhile to point out that the $g_{r_s r_s}$ component of the metric is not identical to zero; while if one were to write the Schwarzschild metric in the corresponding coordinates (u, r_T, θ, ϕ), where r_T is the tortoise coordinate, one would obtain $g_{r_T r_T} = 0$. The point is that in Schwarzschild case, demanding $du = 0$, $d\theta = 0$ and $d\phi = 0$, characterizes outgoing null geodesics; but in Kerr spacetime this is not the case, so that an increment of r_s, maintaining the other three coordinates constant, provokes a motion on the null hypersurface u =constant, but not along a null direction.

3 Null coordinates in regions II and III

To understand how to define smooth functions at the Cauchy horizons, let us study the behavior of the null functions in a neighborhood of C_R and of C_L (See figure 2.). We will begin with the study of v_{II} in a neighborhood of C_R, along the null geodesics contained in the congruence u_{II} =constant.

One can see that in region II dt_{II} plays the role of a spacelike one form, while dr_s has the role of a timelike one form that grows towards r_- in the causal diagram 2. So that the relations between the null functions u_{II} and v_{II} with the interior Boyer-Lindquist coordinate system $(t_{II}, r, \theta, \phi_{II})$ is given by

$$du_{II} = -\, dt_{II} + dr_s = -\, dt_{II} + \frac{\sqrt{\mathcal{R}}}{\Delta} dr + k\, d\theta, \tag{33}$$

where we are using dr_s as given by (29) and

$$dv_{II} = dt_{II} + dr_s = \, dt_{II} + \frac{\sqrt{\mathcal{R}}}{\Delta} dr + k\, d\theta; \tag{34}$$

so that in the causal (u_{II}, v_{II}) diagram of region II, one also has that u_{II} increases to the upper left and v_{II} increases to the upper right.

It is useful to remark that in order to obtain the metric in the $\{u_{II}, v_{II}, \theta, \phi\}$ coordinate system one has to replace in (15): $(du \to -du_{II})$ and $(dv \to dv_{II})$.

We can now proceed with the main purpose of this part, which is to define a regular function $\tilde{V}$ in the vicinity of the Cauchy horizon C_R $(r = r_-)$. Let us start by studying the behavior of v_{II} along the null geodesics contained in the congruence u_{II} =constant, which is determined by

$$\dot{v}_{II} = 2\frac{\sqrt{\mathcal{R}}}{\Delta}\dot{r} + 2k\,\dot{\theta} = -2\frac{\mathcal{R}}{\Delta\Sigma} - 2\frac{k^2}{\Sigma}. \tag{35}$$

Note that in this congruence one has that $\dot{r} = -\frac{\sqrt{\mathcal{R}}}{\Sigma}$ and $\dot{\theta} = -\frac{k}{\Sigma}$.

To see the behavior of the first term as a function of the affine parameter λ, let us recall that at the Cauchy horizon C_R one has $-\frac{\Sigma(r_-,\theta)dr}{\sqrt{\mathcal{R}(r_-)}} = d\lambda$; so that, approaching the Cauchy horizon C_R in region II, to first order one has

$$\Delta = (r - r_+)(r - r_-) = \frac{\sqrt{\mathcal{R}(r_-)}}{\Sigma(r_-,\theta)}(\lambda - \lambda_-)(r_+ - r_-) + \mathscr{O}((\lambda - \lambda_-)^2); \tag{36}$$

with $\lambda < \lambda_-$. Then, the integration of the divergent term of (35), close to the Cauchy horizon C_R, is

$$-2\frac{(r_-^2 + a^2)^2}{\Delta\Sigma(r_-,\theta)}d\lambda = -\,2\frac{(r_-^2 + a^2)^2}{(r_+ - r_-)\sqrt{\mathcal{R}(r_-)}}\frac{d\lambda}{(\lambda - \lambda_-)} = -2\frac{(r_-^2 + a^2)}{(r_+ - r_-)}\frac{d\lambda}{(\lambda - \lambda_-)} = -\frac{d\lambda}{\kappa_-(\lambda - \lambda_-)}; \tag{37}$$

where

$$\kappa_- = \frac{(r_+ - r_-)}{2\sqrt{\mathcal{R}(r_-)}} = \frac{(r_+ - r_-)}{2(r_-^2 + a^2)} = \frac{\sqrt{m^2 - a^2}}{2mr_-}; \tag{38}$$

which we call κ_- because of its analogy with κ_+. This means that in this asymptotic region one has $v \approxeq \frac{-1}{\kappa_-}\ln(\lambda_- - \lambda)$. So that the function that cures this logarithmic behavior must be an exponential; for this reason we define

$$\tilde{V} = -\exp(-\kappa_-\, v_{II}); \tag{39}$$

which by construction, satisfies, as one approaches the Cauchy horizon C_R, along the null geodesics contained in the null congruence U =constant, that

$$d\tilde{V} \approx d\lambda. \tag{40}$$

Similarly, we also define

$$\tilde{U} = -\exp(-\kappa_-\, u_{II}); \tag{41}$$

which, for analogous reasons, is a regular null function close the Cauchy horizon C_L.

The behavior of u_{II}, v_{II} near $r = r_-$ is

$$\lim_{r\to r_-, v=v_0} u_{II} = \infty, \tag{42}$$

$$\lim_{r\to r_-, u=u_0} v_{II} = \infty. \tag{43}$$

which is consistent with our definitions (39) and (41).

It is important to remark that with these definitions we obtain the same metric functional expression as (23) and (24), with the only difference being that in region II, one has to choose $(\kappa = \kappa_-)$, $(\pm_{pf} = -)$ and take an opposite sign in $g_{U_{II}\theta}$, $g_{U_{II}\varphi}$, $g_{V_{II}\theta}$ and $g_{V_{II}\varphi}$.

Note that to cover regions I and II with null functions that are smooth across H_f and C_R, one can use the set $(U, \tilde{V})$; which we plan to employ below.

We can define

$$\tilde{U}_{\text{compact}} = \arctan(\tilde{U}), \tag{44}$$

$$\tilde{V}_{\text{compact}} = \arctan(\tilde{V}); \tag{45}$$

and extend the definitions of ψ and ξ, as used by Carter[8], accordingly. In this way we can explicitly construct a conformal diagram where each point represents a fixed value of the pair $(\tilde{U}_{\text{compact}}, \tilde{V}_{\text{compact}})$ or equivalently, of the pair $(\tilde{U}, \tilde{V})$. It is clear that this technique can be performed in each region.

In region III, each one-form dt_a and dr_a, recovers the same causal character as of region I, but with the difference that r and r_s decreases to the right. Therefore, we can use a similar definition

$$du_{\text{III}} = dt_{\text{III}} + dr_s, \tag{46}$$

$$dv_{\text{III}} = dt_{\text{III}} - dr_s. \tag{47}$$

Then, to build the null tetrad we take $\ell_{\text{III}} = du_{\text{III}}$, $n_{\text{III}} = \frac{\Sigma\Delta}{2\Upsilon} dv_{\text{III}}$, completing the tetrad in an analogous way, as we did previously; namely, m^a_{III} is tangent to the surfaces r_s=constant, and the usual null tetrad metric conditions are satisfied. In this case, for each surface r_s =constant, we also obtain the same functional expressions of Extrinsic and Gaussian curvature.

It is useful to remark that in order to obtain the metric in the $\{u_{\text{III}}, v_{\text{III}}, \theta, \phi\}$ coordinate system one has to replace in (15): $(du \to dv_{\text{III}})$ and $(dv \to du_{\text{III}})$.

Note also that the functional expressions of $\tilde{U}$ and $\tilde{V}$ are good coordinates for region III.

4 Conformal diagram at the axis of symmetry

Let us note that at the axis of symmetry, the right hand side of equation (8) is zero, so that $k = 0$ and $K = 0$ along the axis. Therefore, the calculation of the null functions at the axis is trivial.

Once one has the appropriate definition of the extended coordinates, the causal diagram of figure 2 is straightforward to construct; following the ideas already presented in [8].

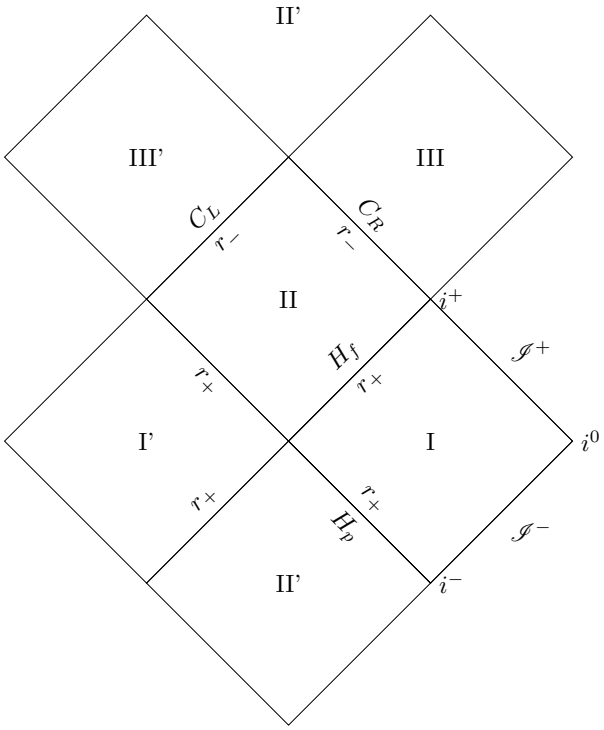

Figure 2: Carter conformal diagram of Kerr spacetime at the axis of symmetry. One can extend in a natural way this diagram to future and past regions.

In region I, we can take Carter functions $\psi = U_{\text{compact}} + V_{\text{compact}}$ and $\xi = V_{\text{compact}} - U_{\text{compact}}$, where we can define

$$U_{\text{compact}} = \arctan(U), \tag{48}$$
$$V_{\text{compact}} = \arctan(V). \tag{49}$$

The conformal diagram shown in figure 2 is constructed by taking (ξ, ψ) as horizontal and vertical coordinates respectively.

To extend the diagram to future and past regions, one has to deal with the analog coordinates to U and V so that they are smooth across the corresponding horizons, as we have described.

In the following sections we present conformal diagrams that have meaning away from the axis of symmetry.

Since the construction of conformal diagrams is rather difficult, some authors have tried other techniques, as in [17]; where they have introduced projection diagrams.

5 Global conformal diagram with timelike trajectories

5.1 On global conformal diagrams

We can see then that one of the great benefits of having constructed a double null coordinate system in Kerr spacetime is that one can now describe its causal structure. Recall that up to now, the conformal diagrams were well understood only at the axis, namely for $\theta = 0$ or $\theta = \pi$; as it is depicted in diagram (a) of figure 1 in [8], or in figure 27 of page 312 in [9], or in figure 2. However, our construction allows us to extend the validity of those causal diagrams, where now each point represents the intersection of the null coordinates. For instance, the intersection of the null hypersurface u =const. with the null hypersurface v =const., determines a particular topological sphere with r_s =constant. On these surfaces, the radial coordinate r has a small range of variability, but the angular coordinates θ and φ vary across their whole respective range of $[0, \pi]$ and $[0, 2\pi]$. This is why we emphasize the word global in our conformal diagrams. As an example of the typical small variations of the coordinate r along the surfaces r_s=constant we can observe for instance Figure 1. There, one can notice that when reaching the Equatorial plane, along the r_s=constant surface, the r function is a little bit smaller than 3, which is the value at the axis; and in fact numerically we can calculate that it has the value $r = 2.960$ at the Equatorial plane. Using the coordinates U and V that allow us to cross the future horizon $H = H_f$, one has the same property; so that we can give general validity to the causal diagrams using these type of null coordinates. In other words, we can construct conformal diagrams as the one shown in figure 2, where each

point corresponds to particular values of each of the null coordinates. Alternatively, each point represents a topological sphere which could be at one of the horizons with $r = r_+$ or r_-, or the sphere has r_s =constant; recalling that r_s diverges at the horizons, where $\lim_{r\to r_+} r_s = -\infty$ and $\lim_{r\to r_-} r_s = \infty$. The set r_s =constant, is a 2-dimensional spacelike surface family(in region I), that corresponds to a well behaved function $r(\theta)$ in terms of Boyer-Lindquist coordinates.

Note that the regular function on C_R is $\tilde{V}$; which therefore can also be used in region III. Then, since we would like to draw curves that go from region I to region II and also to region III, it is more convenient to use for all these three regions the definitions:

$$\psi = U_{\text{compact}} + \tilde{V}_{\text{compact}} = \arctan(U) + \arctan(\tilde{V}), \tag{50}$$

and

$$\xi = \tilde{V}_{\text{compact}} - U_{\text{compact}} = \arctan(\tilde{V}) - \arctan(U). \tag{51}$$

Then, in this case, the future horizon H_f is characterized by the condition $U = 0$, or equivalently the line $\psi = \xi$, from $-\frac{\pi}{2}$ to 0. While the boundary C_R is characterized by the line $\psi = -\xi$, again for ξ in the range $[-\frac{\pi}{2}, 0]$. The origin is thus set at i^+.

5.2 Computing the plot of timelike trajectories in a conformal diagram

In order to show the utility of having an explicit construction of a conformal of Kerr spacetime we compute here the plot of three timelike curves in such diagram.

The three timelike curves are defined in the following way. The starting point is to consider the timelike geodesic equations for the coordinates $(\tilde{V}, r, \theta, \varphi)$; which are a set of first order differential equations. This set of equations involves the requirement that the curve be timelike. Then, although we start from the geodesic equations, we transform them in order to generate timelike curves which are not geodesics. In the equation involving $\tilde{V}$, the knowledge of the function K is required; but instead of this, we use $K_0 = \frac{(r^2+a^2)a^2\sin(\theta)^2}{(r^2+a^2\sin(\theta)^2)}$, which is the limit of the function K when the mass of the spacetime is taken to be very small. This provides then for a recipe to calculate a timelike curve which for $m \neq 0$ is not a geodesic. Although we require in one of the equations that these curves are timelike, they cease to be geodesic, because for geodesics one should use K instead of K_0, that we employ. The reason to calculate these timelike trajectories instead of the geodesics, is to facilitate the numerical calculations, since to attain a reasonable precision in the trajectories would require high accuracy in the calculation of K along each point used by method of integration as those of Runge-Kutta type. We also compute U numerically.

Orbit 1 is calculated with $L_z = 0.2$, $E = 1.2$ and $K_g = \delta_g a^2\cos(\theta_c)^2 + (Ea\sin(\theta_c) - L_z/\sin(\theta_c))^2$ with $\theta_c = \frac{\pi}{6}$ and $\delta_g = 1$ for a timelike curve. Orbit 2 uses the constants above but with $E = 0.5$. While orbit 3 is like orbit 2 but with $L_z = 0.7$. All curves pass through the point: $\tilde{V} = \tan(-\frac{\pi}{4})$, $U = 0$, $\theta = \frac{\pi}{4}$ and $\varphi = 0$.

The graph in figure 3 shows the numerically calculated drawing of these three curves in the conformal diagram.

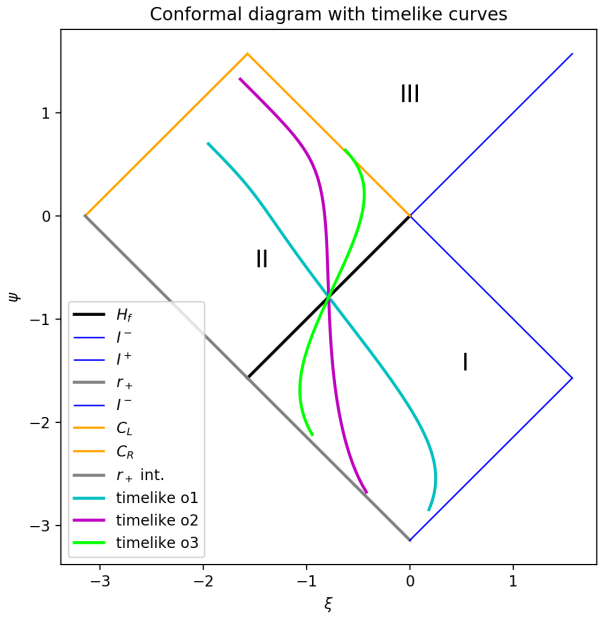

Figure 3: Conformal diagram showing three timelike curves. We use colors in this graph to denote horizons and infinities. The blue lines denote future and past null infinites. The yellow lines denote the Cauchy horizons, where $r = r_-$. The gray lines denote the horizons, where $r = r_+$. The three timelike curves are drawn in cyan, magenta and green.

We would like to emphasize that the design of these three timelike curves was chosen just because of numerical convenience. But even so, the calculations demanded some efforts on the fourth order Runge-Kutta integrators. Thus we tried to extend the range as much as possible. The technique to select them was to fix a point in the $U = 0$ surface, that is at the future event horizon; and then to pick up three initial conditions covering a fast 'inward' infall, orbit 1, a normal timelike behavior, orbit 2, and a fast 'outward' also infall, orbit 3. We call 'inward' a motion with increasing U behavior, and 'outward' a motion with increasing $\tilde{V}$ behavior; which in the graphs are approximate motions to the left and to the right respectively. It can be seen in Figure 3 that the timelike trajectory o3 touches the Cauchy horizon C_R; and it actually enters into region III, but far away from the problematic noncausal zone inside region III. We have tried several initial conditions until we found one whose trajectory enters region III. One should notice that the spacetime is smooth across C_R and that geodesics and smooth timelike curves, as o3, can cross the Cauchy horizon.

It is immaterial which are the three timelike curves; what is important is that one can use a numerical program to draw the graph of these curves in the conformal diagram. This is only possible if one has the explicit construction of the conformal diagram, as we present here.

6 The extraordinary noncausal region III$_b$

6.1 On the sign of Υ

In his original article Kerr[16] presented the metric also in what is now know as the Kerr-Schild[18] form. Then Boyer and Lindquist[12] used this form of the metric to express their Boyer-Lindquist coordinates; from which it is clear that increasing the value of the angular coordinate ϕ in 2π implies traveling around in a closed loop in the manifold. Since the sign of $g_{\phi,\phi}$ is determined by Υ, in the regions where Υ is negative, one has closed timelike curves, and the causal character of dt and dr_s changes. All of this occurs inside region III; where we were using (46) and (47), and more specifically in a sector within the zone $r < 0$.

The region where $g_{\phi,\phi}$ becomes positive, equivalently Υ change its sign, is depicted in the following figures.

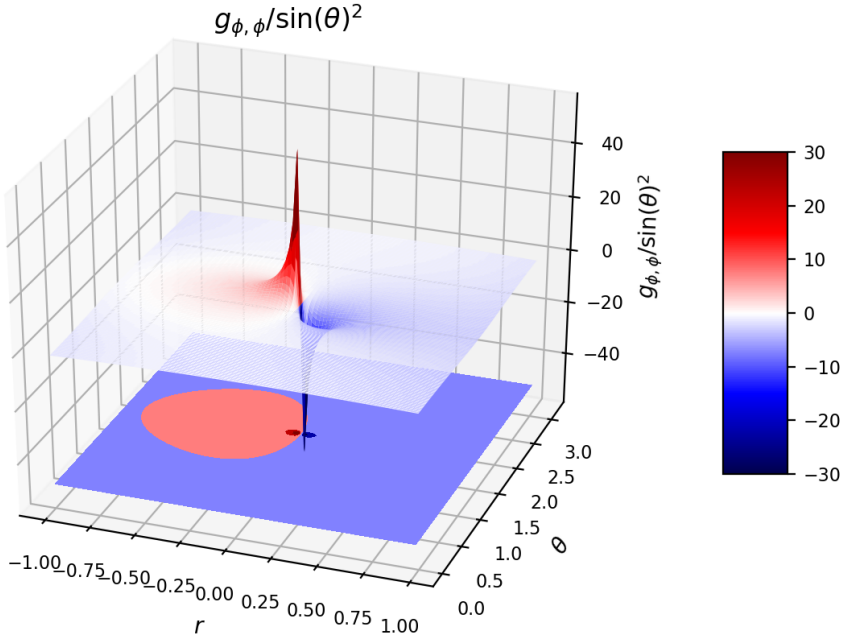

Figure 4: Three dimensional graph of the sign of $g_{\phi,\phi}$.

Let us observe that

$$u_{\rm III} - v_{\rm III} = 2r_s = \frac{1}{\kappa_+}\ln(U) - \frac{1}{\kappa_-}\ln(\tilde{V}) = \ln(U^{\frac{1}{\kappa_+}}) - \ln(\tilde{V}^{\frac{1}{\kappa_-}}) = \ln\left(\frac{U^{\frac{1}{\kappa_+}}}{\tilde{V}^{\frac{1}{\kappa_-}}}\right); \tag{52}$$

or

$$U = \tilde{V}^{\frac{\kappa_+}{\kappa_-}}\exp(2\kappa_+ r_s). \tag{53}$$

One extreme of the noncausal region is at $r = 0$ and $\theta = \frac{\pi}{2}$; that is, at the ring singularity. Then, performing the numeric integration of $\int_0^{\frac{\pi}{2}} k(r=0,\theta)d\theta$ we obtain $r_{s0} = \int_0^{\frac{\pi}{2}} k(r=0,\theta)d\theta = 0.66078$; so that one has

$$U_0 = \tilde{V}^{\frac{\kappa_+}{\kappa_-}}\exp(2\kappa_+ r_{s0}). \tag{54}$$

The other extreme of the noncausal regions is for approximately $r_1 = -0.9$, and $\theta = \frac{\pi}{2}$; so that $r_{s1} = r_1 + \frac{2mr_+}{r_+-r_-}\ln(1-\frac{r_1}{r_+}) - \frac{2mr_-}{r_+-r_-}\ln(1-\frac{r_1}{r_-}) + \int_0^{\frac{\pi}{2}} k(r_1,\theta)d\theta$. However, at the moment we do not have a numeric calculation of k for negative values of r, so we estimate $\int_0^{\frac{\pi}{2}} k(r_1,\theta)d\theta$ with the above value of r_{s0}. In this way, for the other extreme one has

$$U_1 = \tilde{V}^{\frac{\kappa_+}{\kappa_-}}\exp(2\kappa_+ r_{s1}); \tag{55}$$

with the approximate value $r_{s1} = 0.1651$.

So, the natural question is, can one define a continuous $u_{{\rm III}_a}$ and $v_{{\rm III}_a}$ null coordinates inside the noncausal region ${\rm III}_b$? In order to construct the null functions in some region, we need to have the function K or k in that region. It happens that the partial differential equation that K or k must satisfy, has problems when Υ becomes negative, because as we show below the argument in the left square root of equation (6) becomes negative. More concretely, the null geodesic congruence that we are using, ceases to be integrable. That is, we can not carry out the construction inside the noncausal region. Moreover, any such construction that relies on a null congruence coming from null infinity, will have the same fate. In other words, these type of constructions are not able to provide a continuous set of null coordinates that enter the noncausal region. In fact, since it is a noncausal region, it would be unnatural to think that there exists a mechanism such that this type of construction can be carried out at all.

All these means that the interior of the noncausal region ${\rm III}_b$ can not be represented in a global conformal diagram of Kerr spacetime.

This point has not been mentioned previously in the literature.

6.2 On the construction of the null congruence

In the previous subsection we have indicated that due to the nature of the calculation of the function K, one can deduce that our construction for a double null coordinate system can not be extended to the noncausal

region III_b. In this subsection instead we will concentrate on the problems related to the construction of the null geodesic congruence, that we employ in our construction. That is, we will consider each geodesic at a time, where K is constant along each of them.

The existence of a noncausal region poses the question of what is the extent in the spacetime where one can construct the reference null geodesic congruence.

First of all, it is worthwhile to recall that Carter has shown in [19] that in extending the manifold to the future and to the past, one repeatedly encounters regions of type I, II and III, in an arrangement shown in Figure 2. In particular all regions of type III have the same geometrical properties. For this reason, in this subsection we will concentrate on the region of type III which can be reached with past directed null geodesics emanating from future plus infinity I^+.

To study the behavior of the null geodesics let us concentrate in the r and θ motion, which are the coordinates used by Kerr[16] and Boyer and Lindquist[12].

The r motion is given by:

$$\Sigma^2 \dot{r}^2 = \left[E(r^2+a^2) - aL_z\right]^2 - K\Delta \equiv \mathcal{R}_{L_z E}; \tag{56}$$

where we have taken the opportunity to define $\mathcal{R}_{L_z E}$. The θ motion is given by:

$$\Sigma^2 \dot{\theta}^2 = K - \left[Ea\sin(\theta) - \frac{L_z}{\sin(\theta)}\right]^2 \equiv \Theta_{L_z E}, \tag{57}$$

which invites us also to define the function $\Theta_{L_z E}$ as above. For our congruence we need to consider $L_z = 0$, and without loss of generality, we take $E = 1$. Under these conditions we have that the right hand side of (56) becomes

$$\mathcal{R}_{01} = (r^2+a^2)^2 - K\Delta = \Upsilon - \Delta\Theta_{01}; \tag{58}$$

since

$$\Theta_{01} = K - a^2\sin(\theta)^2. \tag{59}$$

Let us note that due to the nature of the θ motion equation, one must have $\Theta_{01} \geqslant 0$, and that in the interior of region III one has $\Delta > 0$. In (58) we have rearrange terms so that Υ appears explicitly. Since Υ becomes negative in the noncausal region III_b, one can see that $\mathcal{R}_{01}$ turns negative in this region, and therefore indicates that a geodesic coming from outside this zone will not be able to enter into it.

Let us see this in more detail by studying the behavior of (58) with $K = a^2\sin(\theta_\infty)^2$, which is shown in the next graph. That is, let us study the null geodesics that we use to build the double null coordinate system; which start at future null infinity, where θ_∞ is the value of coordinate θ at this asymptotic boundary. To facilitate the presentation we use in the graph the notation $\theta_\infty = \delta\pi$, that is we express θ_∞ in terms of the more convenient parameter δ.

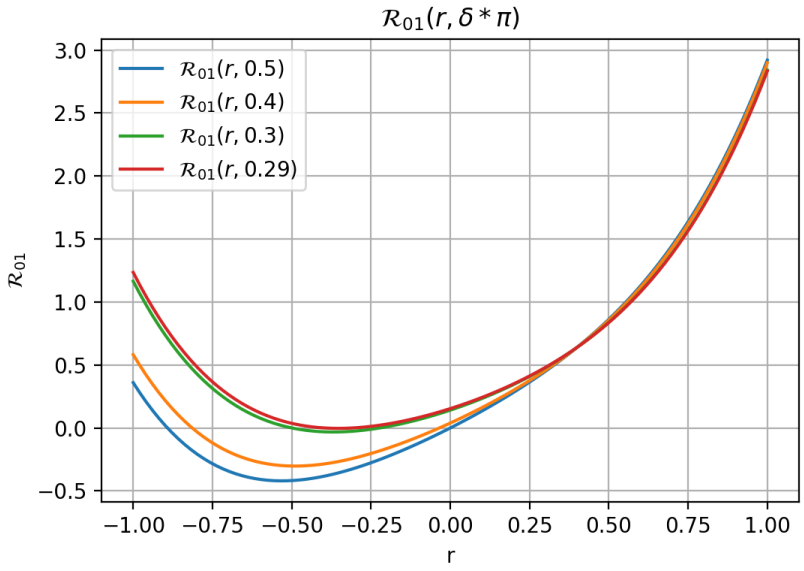

Figure 5: $\mathcal{R}_{01}(r, \delta * \pi)$ for $\delta = 0.5$, 0.4, 0.3 and 0.29; where it shows negative values as function of r.

We would like to emphasize that the choice $E = 1$ is just done for simplicity and does not represent a restriction, in particular, one can easily see that in the general case, $K' = K/E^2$ satisfies equation (6). It can be seen that for $\delta^\diamond \approx 0.289 < \delta < 0.5$ one has that R_{01} shows negative values for some r's that are negative and greater than -1. At this point it is worthwhile to recall that Carter[19] has shown that only the geodesics that strike the singularity are incomplete. Therefore, a null geodesic that reaches a point where $\mathcal{R}_{01}$ becomes negative, as for example is the case for the null geodesic starting with $\delta = 0.4$, will not stop there, but will reverse its r motion. That is, in the previous motion one had $\dot{r} < 0$, and after the point in which $\mathcal{R}_{01} = 0$, one will have $\dot{r} > 0$. In other words, one therefore deduces that for the chosen geometrical parameters m and a, the null geodesics coming from future null infinity, with values of δ in the range shown in the graph, will invert the r motion to greater values; with the exception of the critical value of $\delta^\diamond$ where $\mathcal{R}_{01}$ shows a double root. This situation is analog to the discussion in classical mechanics of the motion of one particle with conserved quantities; where for fixed δ, the radial potential energy would be $-\mathcal{R}_{01}(r, \delta\pi)$ and the mechanical energy is zero. Note that there is an equatorial symmetry with respect to this effect.

Also, it is observed that for $\delta \lessapprox 0.289$, the null geodesics in our congruence, coming from future null infinity will continue to the asymptotic region $r \to -\infty$; so that one can construct our congruence in the neighborhood of the axis of symmetry. Let us note that the extreme $\theta^\diamond = \delta^\diamond \pi$ has been estimated for the case $m = 1$ and $a = 0.8$. These limiting values can be calculated solving a cubic equation for $r^\diamond$ and then calculating $\theta^\diamond$; which are deduced from $\mathcal{R} = 0$ and $\frac{d\mathcal{R}}{dr} = 0$.

It should be noticed that for the geodesics with parameter δ in the range $\delta^\diamond \leq \delta \leq 1 - \delta^\diamond$, they will cease to form a hypersurface after the turning points, because from there they will inevitably cross other geodesics in the congruence; which can also be checked by noticing that the spin coefficient ρ, which is related to the divergence of the congruence, blows up when $\mathcal{R}$ goes to zero[13]. Of course the special case is $\delta = 0.5$, which are the geodesics that reach the singularity.

In summary, our construction for a double null coordinate system can not be extended to region III_b. Therefore, the noncausal region can not be represented in the conformal diagrams.

6.3 Calculation of the function k

We have been able to integrate k, for all values of θ, up to $r = 0$, as it is shown in the next graph.

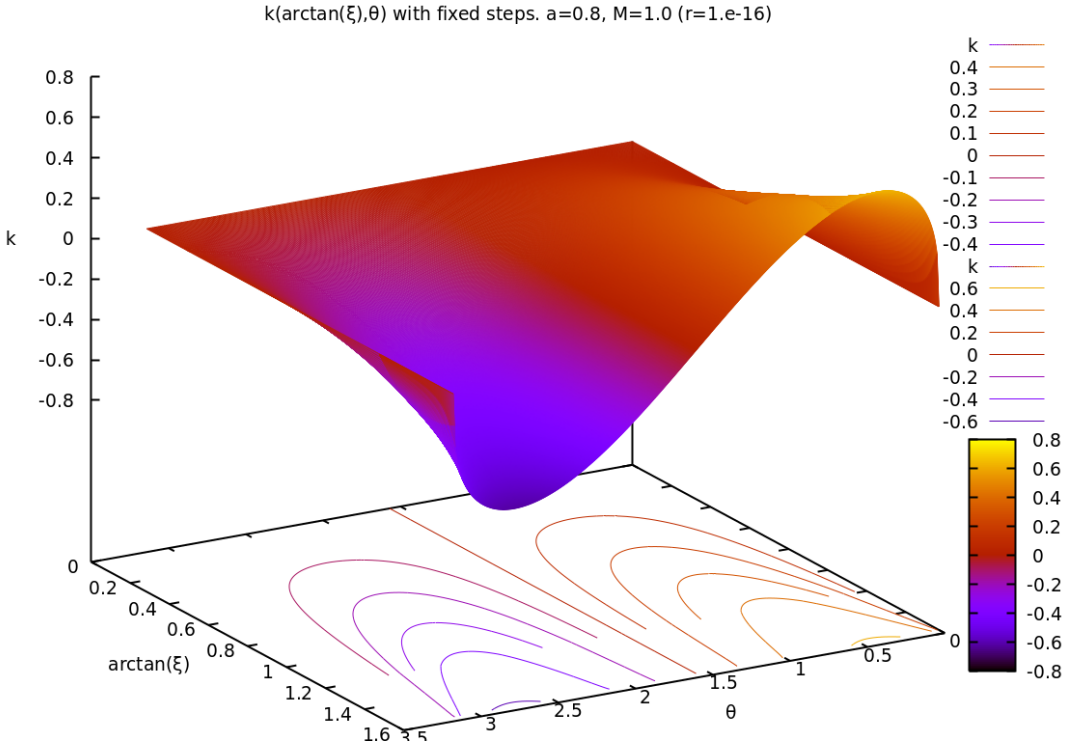

Figure 6: Numerical solution of k in terms of the coordinates (ξ, θ).

In figure 6 it is shown the graph of the numerical integration of k from $r = \infty$ up to $r = 10^{-16}$; which indicates a smooth behavior of the function for positive r.

7 General conformal diagram of regions I, II and III

The existence of the extraordinary noncausal zone b in region III poses a number of questions on the physical reality of the whole region III. As Carter has pointed out[19], one can have closed timelike lines that extend to any part of region III. It is outside the scope of this work to review the studies on the global causal structure of Kerr spacetime; instead, we would like to present a useful tool that helps to carryout those studies.

An explicit conformal diagram of the three regions I, II and III is presented here.

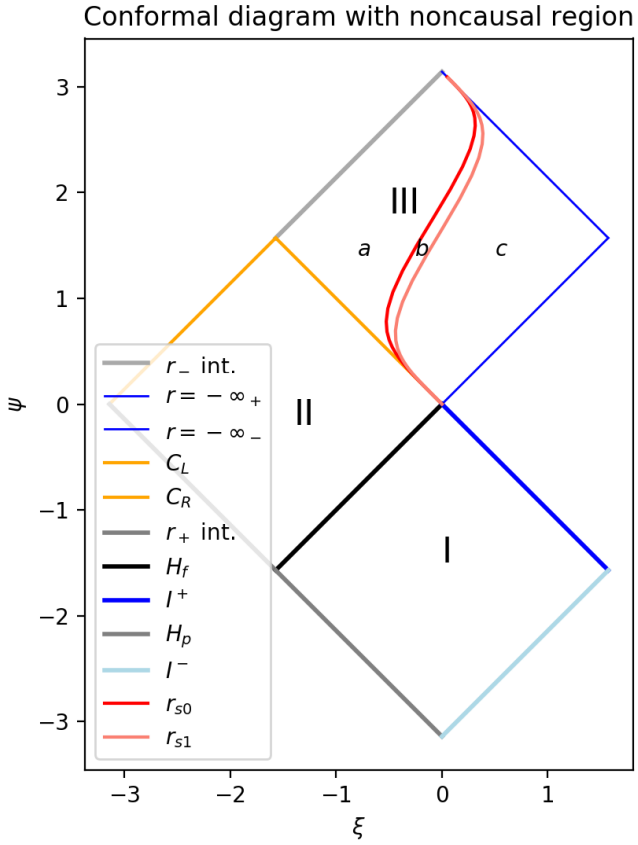

Figure 7: Conformal diagram of the three immediate regions. Region III is subdivided in zones a, b and c. Note that the red line denotes the boundary of the noncausal region, and the ring singularity. The reason for the curly shape of these curves is that one regular coordinates uses κ_+ in its definition and the other uses κ_-; as explained in the text. We denote with 'r_- int' the line in the conformal diagram indicating the value $r = r_-$ in the interior region III, to distinguish it from the Cauchy horizon C_R which also satisfies $r = r_-$. We denote with $r = -\infty_+$ and $r = -\infty_-$ the asymptotic regimes of region III, for $r \to -\infty$, to the future and to the past respectively. The notation C_L and C_R was introduced before in the text. We denote with 'r_+ int' the line in the conformal diagram denoting the value $r = r_+$ in the interior region II, to distinguish it from the future horizon H_f, defined previously. We use I^+ to denote future null infinity of the physical region I. We use I^- to denote past null infinity of the physical region I. H_p is used as before to denote the past horizon of the black hole. As explained in the text, we denote with r_{s0} the value of r_s at the ring singularity, where the value of the r coordinate is 0. Also, we use r_{s1} to denote the value of r_s at the extreme of the noncausal region, for the smallest value of the coordinate r; estimated to be around -0.9 for our choice of geometrical parameters m and a. The region III_a correspond to points in region III where the radial coordinate is larger or equal than zero, $r \geqslant 0$. The region III_c correspond to the points in the zone of region III where $r < 0$ and are outside of the noncausal region III_b. As explained, region III_b can not be drawn in the conformal diagram, but we can draw the line corresponding to the largest value of r, and the line corresponding to its smallest value in the noncausal region.

Region III_a is the zone of region III where $r_- \geqslant r \geqslant 0$.

We have noticed before that the noncausal region III_b can not be represented in a global conformal diagram of Kerr spacetime. However we can draw in the conformal diagram, the lines corresponding to the largest and smallest radius in the boundary of the noncausal region. Those are the red and salmon lines in the graph of figure 7 . The b in the graph, is just to indicate that the red and salmon lines are extreme points of the noncausal region. It should be emphasized however that other points, outside the noncausal region, might be drawn in the conformal diagram into the two dimensional area in the graph between the red and salmon lines. This is expected, since one is dealing with a four dimensional spacetime, but one is drawing two dimensional conformal diagrams. In fact, recall that for regular regions, as those of type I and II, all points in a particular sphere r_s =constant, are plotted in the same point in the conformal diagram.

The zone c is the zone of region III where r is negative and outside the noncausal region. We denote this as the region III_c.

The bottom line is that the topological causal properties of the four dimensional manifold can be deduced from the structure of the conformal diagram that we have just introduced. Therefore, since in region III one is missing the noncausal zone, the topology implied by the original Carter conformal diagram at the symmetry axis, can not be extended to the global spacetime. This subtle point is generally missed, since even in textbooks[20], the introduction of conformal diagrams of Kerr spacetime do not mention this issue. In fact in those diagrams, one can not draw timelike curves, not even the ring singularity with precision, since the authors do not have or provide, the set of needed double null coordinates that would allow for those drawings. We solve this situation with our present work.

8 Final comments

In this article, we have presented for the first time, an explicit construction of a conformal diagram for the spacetime of a black hole with angular momentum, which is valid globally; as opposed to the previous ones that where only valid at the axis of symmetry.

We have shown how to define appropriate smooth null coordinates across outer and inner horizons, so that our construction allows us to extend these diagrams to the complete spacetime, where now each point represents the intersection of the null coordinates.

All previous findings on the global causal structure of Kerr spacetime[19] can be reproduced with our choice of double null coordinates, of type (u, v) and of type (U, V); with the advantage that now we can visualize this structure through the global conformal diagrams as that of figure 7. Although we have concentrated in this article in regions I, II and III, it is clear that our construction can be naturally extended to the maximal analytic manifold[12]; so that we give meaning to diagrams of the type shown in figure 2 outside of the axis of symmetry.

Previous presentations of conformal diagrams of the extended Kerr geometry[20, 21] were of qualitative nature and were not able to calculate in the graph specific curves or regions. For instance, the graphs in figures 11.7 and 11.8 of [21] are not 'global conformal diagrams' since they are constructed from demanding that two coordinates are maintained fixed; so that the curves we computed in this work can not be drawn on those diagrams. In particular, in [21] the authors erroneously state, copying an error from the MTW textbook[22], that their function v is null, (which in [22] is called $\tilde{V}$). Since we use these symbols in our article we rename their function to v^K, since Kerr used the retarded version of it. Then one can readily calculate that $g^{ab} dv^K_a dv^K_b = -\frac{a^2 \sin(\theta)^2}{r^2 + a^2 \cos(\theta)^2}$; which is different from zero at generic points, and therefore indicates that it is not a null coordinate. Note that the contraction is zero at the axis of symmetry. In the MTW textbook the error appears in point E3, in page 880 of the 1973 edition. This mistake might be the source of the general belief in the community that Kerr spacetime was almost as easy as Schwarzschild one. But in fact, the subtleties of Kerr geometry makes all discussions much more difficult. A confusing fact, for example, is that the function v^K contains the geodesics defining the principal null directions; but this null congruence has twist and therefore does not define a null function. For this reason in [13] we dealt with a null congruence without twist, that allowed us to define our pair of null coordinates for Kerr spacetime.

In contrast to this, our explicit construction of conformal diagrams for Kerr spacetime, has permitted us here to numerically draw arbitrary curves, as those shown in figure 3, and the boundary of the noncausal region, depicted in figure 7 .

The possibility to construct these type of global conformal diagrams contributes to the visual understanding of the global structure of the spacetime.

Acknowledgments: We are very grateful to István Rácz for comments and questions that have helped us to improve the presentation of an early version and to Emanuel Gallo for several suggestions and corrections

and to Jack Davies for proof reading. We would like also to thank two anonymous Referees, since through the interaction with them we were able to improve considerably the presentation of the article.

We acknowledge support from CONICET, SeCyT-UNC and FONCYT.

References

[1] P. T. Chrusciel, J. Lopes Costa, and M. Heusler, "Stationary Black Holes: Uniqueness and Beyond," *Living Rev. Rel.* **15** (2012) 7, arXiv:1205.6112 [gr-qc].

[2] **LIGO Scientific, Virgo** Collaboration, B. P. Abbott *et al.*, "Observation of Gravitational Waves from a Binary Black Hole Merger," *Phys. Rev. Lett.* **116** no. 6, (2016) 061102, arXiv:1602.03837 [gr-qc].

[3] **LIGO Scientific, Virgo** Collaboration, B. P. Abbott *et al.*, "Properties of the Binary Black Hole Merger GW150914," *Phys. Rev. Lett.* **116** no. 24, (2016) 241102, arXiv:1602.03840 [gr-qc].

[4] **Event Horizon Telescope** Collaboration, K. Akiyama *et al.*, "First M87 Event Horizon Telescope Results. IV. Imaging the Central Supermassive Black Hole," *Astrophys. J.* **875** no. 1, (2019) L4.

[5] **Event Horizon Telescope** Collaboration, K. Akiyama *et al.*, "First Sagittarius A* Event Horizon Telescope Results. III. Imaging of the Galactic Center Supermassive Black Hole," *Astrophys. J. Lett.* **930** no. 2, (2022) L14.

[6] E. F. Boero and O. M. Moreschi, "Strong gravitational lens image of the M87 black hole with a simple accreting matter model," *Monthly Notices of the Royal Astronomical Society* **507** no. 4, (08, 2021) 5974–5990.

[7] B. Carter, "Black hole equilibrium states," in *Black holes*, C. DeWitt and B. DeWitt, eds. Gordon and Breach Science Pu., 1973.

[8] B. Carter, "Complete Analytic Extension of the Symmetry Axis of Kerr's Solution of Einstein's Equations," *Phys. Rev.* **141** (1966) 1242–1247.

[9] S. Chandrasekhar, *The mathematical theory of black holes.* Oxford University Press, 646 p., 1983.

[10] M. Walker, "Block Diagrams and the Extension of Timelike Two-Surfaces," *J.Math.Phys.* **11** (1970) 2280–2286.

[11] S. Hawking and G. Ellis, *The large scale structure of space-time.* Cambridge University Press, 1973.

[12] R. H. Boyer and R. W. Lindquist, "Maximal analytic extension of the Kerr metric," *J.Math.Phys.* **8** (1967) 265–281.

[13] M. A. Argañaraz and O. M. Moreschi, "Double null coordinates for Kerr spacetime," *Phys. Rev. D* **104** no. 2, (2021) 024049.

[14] O. M. Moreschi, "Intrinsic angular momentum and center of mass in general relativity," *Class.Quantum Grav.* **21** (2004) 5409–5425.

[15] E. Gallo and O. M. Moreschi, "Intrinsic angular momentum for radiating spacetimes which agrees with the Komar integral in the axisymmetric case," *Phys.Rev.* **D89** (2014) 084009, arXiv:1404.2475 [gr-qc].

[16] R. P. Kerr, "Gravitational field of a spinning mass as an example of algebraically special metrics," *PRL* **11** (1963) 237–238.

[17] P. T. Chrusciel, C. R. Olz, and S. J. Szybka, "Space-time diagrammatics," *Phys. Rev. D* **86** (2012) 124041, arXiv:1211.1718 [gr-qc].

[18] R. Kerr and A. Schild, "Republication of: A new class of vacuum solutions of the einstein field equations (1965)," *General Relativity and Gravitation* **41** (10, 2009) 2485–2499.

[19] B. Carter, "Global structure of the Kerr family of gravitational fields," *Phys. Rev.* **174** (1968) 1559–1571.

[20] R. Wald, *General Relativity.* The Chicago University Press, 1984.

[21] J. B. Griffiths and J. Podolský, *Exact Space-Times in Einstein's General Relativity.* Cambridge Univeristy Press, Cambridge, 2009.

[22] C. W. Misner, K. S. Thorne, and J. A. Wheeler, *Gravitation.* No. pt. 3 in Gravitation. W. H. Freeman and Company, 1973. http://books.google.com.ar/books?id=w4Gigq3tY1kC.